Reprinted from November 1981, Vol. 103, Journal of Engineering for Industry

P. K. Venuvinod
Senior Lecturer.
Assoc. Mem. ASME

W. S. Lau
Principal Lecturer.
Mem. ASME

Production and Industrial Engineering Department,
Hong Kong Polytechnic,
Hong Kong

P. Narasimha Reddy
Reader in Mechanical Engineering,
Osmania University,
Hyderabad, India

Some Investigations Into Machining With Driven Rotary Tools

Experimental studies have been conducted with driven rotary tools on various work materials, using specially constructed test rigs. The studies include the effect of rotary speed on the geometry, the kinematics and the mechanics of chip formation. The data are analyzed, using the concept of equivalent angle of obliquity. Hitherto unknown and extraordinary effects on the chip formation have been noted which lead to new modes of rotary machining and the expansion of the scope of rotary machining.

Introduction

Rotary machining is a cutting process in which the cutting edge has a motion along itself which results in a continuous feeding of the cutting edge into the cutting zone. This motion, called the rotary motion, is in addition to the relative motions of cutting speed and feed between the tool and the workpiece.

The rotary tool usually takes the form of a frustrum of a cone, with its axis generally oriented in two different ways relative to the workpiece. This is illustrated in Fig. 1. In type I setting, the tool axis is parallel to the machined surface and makes an angle i with the cutting speed vector V_w. Angle i, the setting parameter of the tool, is equal to the nominal angle of obliquity of the cutting edge. The concept of a nominal angle of obliquity becomes necessary since the actual angle of obliquity varies along the cutting edge. For convenience, the nominal inclination angle is taken as the angle of obliquity i_F of the cutting edge at the point (F) of deepest penetration of the cutting edge into the workpiece. For a type I tool, $i_F = i$. In type II setting, the tool axis makes angles θ_H and θ_V to the normal to the machined surface as shown in Fig. 1. The nominal angle of obliquity i_F in this case is given by the following equation

$$\tan i_F = \frac{\sin \theta_H}{\tan \theta_V} \tag{1}$$

Setting angles θ_H and θ_V modify the rake and clearance angles ν_g and α_g as ground on the tool so that the net nominal normal rake angle is given by:

$$\nu_n = \nu_g - \arccos \theta_H \cos \theta_V \tag{1b}$$

Generally, type II setting is preferable to type I setting in view of the ample space available around the tool axis for designing a tool spindle of adequate stiffness. The workpiece may be fed with normal or reverse feeds as shown in Fig. 1.

Contributed by the Production Engineering Division for publication in the JOURNAL OF ENGINEERING FOR INDUSTRY. Manuscript received at ASME Headquarters October 27, 1980.

The rotary tool may be mounted freely on bearings and allowed to rotate by rolling action with the workpiece. Such a tool is called the self-propelled rotary tool (SPRT). The nominal obliquity i_F determines the tool velocity V_t in this case and is given by:

$$V_t \simeq V_w \sin i_F \tag{2}$$

The selection of i_F is an important problem. In general, it is advisable to restrict the contact angle such that $70 \text{ deg} > i_F > 20 \text{ deg}$.

The rotary motion V_t in this case allows the tool to conduct heat away from the cutting process. Further, the cutting edge has a long cooling period between two short successive cutting periods. Consequently, reductions in cutting temperatures up to 500°C have been observed while machining mild steel [1,2]. The wear rate is therefore significantly reduced. Further, this wear is distributed over a long cutting edge. Thus, the resulting tool life is often thousands of times higher than those obtained using equivalent stationary tools [3,4]. In view of these advantages, the SPRT has been used for machining titanium alloys [5], forgings, welded yokes and laminated packs [6] to advantage. The only limitation is that its application is limited to the production of large and relatively simple surfaces without steps, grooves, etc.

When the rotary tool obtains the rotary motion from an external drive, it is called a driven rotary tool (DRT). The DRT provides greater control on the process since the rotary speed V_t and angle of obliquity i can be chosen at will. Shaw, et al. [7], reported extensive studies on the mechanics of cutting a tube with an orthogonal DRT in the range $V_t/V_w = 0\text{–}2$. By considering all relevant velocities relative to the tool, they established that the process is equivalent to that obtained while machining with a stationary tool of equivalent obliquity given by $i_{eq} = \arctan V_t/V_w$. Some studies on the DRT are available in references [1,8,9]. The present paper briefly reports the results of studies conducted by the authors

on DRT since 1969. V_t/V_w and i_F are varied in a very wide range. It is shown that the rotary speed leads to extraordinary and hitherto unreported changes in the cutting process which are of great theoretical importance in the understanding of metal cutting in general.

Geometric, Kinematic and Force Analysis

Figure 2 illustrates the nature of the geometry, the velocities and the forces involved in free cutting with an oblique DRT. When the tool is stationary, i.e., $V_t = 0$, the chip velocity vector V_c makes an angle $\rho_c (= \rho_{co})$ with the normal to the cutting edge on the rake face. When the tool is given a rotary speed V_t, the rake surface attempts to carry the chip with it and tends to increase the chip velocity V_c and angle ρ_c. The relative velocity vector V_{ct} between the chip and the tool rake is modified. The friction force F at the rake surface, generally, opposes the relative velocity vector V_{ct}. Thus, the force configuration (F_n, F_l, N) at the rake face is modified. Consequent to the changes in the velocity and force configurations at the rake face, the velocity V_s, $(\phi_l)_v$ and force (S_n, S_l, N_s) configurations at the shear plane are to be suitably adjusted to insure compatibility of velocities and equilibrium of the chip. It is thus seen that the rotary speed V_t is capable of significantly influencing the geometry, the kinematics and the mechanics of chip formation. Shaw, et al. [7], have developed an excellent analysis of chip formation associated with free cutting with an orthogonal DRT ($i_F = 0$) using the well-known analyses of conventional oblique cutting. A similar procedure has been applied, in the present case, for analyzing the cutting process associated with an oblique DRT. The relevant equations are given in the Appendix. These equations can be easily developed by applying the procedures given by Shaw, et al. [7], to Fig. 2. The equations are so written as to facilitate the estimation of the relevant parameters from the given or measured parameters of the tool geometry (i_F, ν_n), the cutting conditions (V_w, V_t), the uncut chip dimensions (a, b, l), the chip dimensions (a_c, b_c, l_c), and the cutting force components (P_x, P_y, P_z). The meanings of the various symbols used can be inferred from Fig. 2 and the Nomenclature.

Test Rigs

Test Rig I. This rig was used mainly for investigating the mechanics of rotary cutting under idealized conditions at low cutting speeds and moderate rotary speeds. The work specimens were 6.25mm wide and 100mm long. They were clamped on a three component milling dynamometer using strain gages mounted on four octagonal rings. The dynamometer was mounted on a Heller Milling Machine as shown in Fig. 3. The dynamometer was fitted with a special compensating circuit to cancel out any interactions between channels. A HSS Type II rotary tool was mounted on a specially designed spindle unit. The design of the unit is shown in Fig. 4. The spindle unit was mounted on an angle plate at suitable setting angles θ_H and θ_V with the help of tapered spacers. The rotary drive was obtained from a 0.18 kW (¼hp), 1500 rpm, d-c compound motor through a timing belt drive, a 1:60 reduction unit and another timing belt drive. The speed of the d-c motor was varied by a special circuit to obtain V_t/V_w in a wide range. The work speed was obtained through the longitudinal feed of the table in the range 0–3 m/min. In each case, the chip dimensions (a_c, b_c, l_c) and the cutting forces (P_x, P_y, P_z) were measured. The scratch marks lying in the direction of V_{wt} on the machined surface were studied with a portable microscope so that i_{wt} could directly be measured.

Nomenclature

a = uncut chip thickness
a_c = chip thickness
b = workpiece width
b_c = chip width
F = friction force on the rake surface
F_n, F_l = normal and lateral components of F
i = angle of obliquity, setting angle
i_F = magnitude of the angle of obliquity at the point of maximum penetration of the cutting edge into the workpiece
i_{wt} = angle between the cutting edge and the vector V_{wt}
l = uncut chip length
l_c = chip length
N = normal force on the rake plane
N_s = normal force on the shear plane
P_x = cutting force component normal to P_y and P_z
P_y = cutting force component normal to the machined surface
P_z = cutting force component in the direction of the cutting speed
P_l = cutting force component in the direction of the cutting edge
P_n = cutting force component normal to the cutting edge and P_y
R_n = resultant cutting force in the normal plane
S = shear force on the shear plane
S_n, S_l = normal and lateral components of S
t = depth of cut
U = total cutting power
U_w = cutting power derived from the main drive
U_t = cutting power derived from the rotary tool drive
V_c = chip velocity
V_{ct} = velocity of the chip relative to the rake surface
V_s = shear velocity at the shear plane
V_{sn}, V_{sl} = normal and lateral components of V_s
V_t = rotary velocity of the cutting edge
V_w = work velocity (cutting speed)
V_{wt} = velocity of sliding between the workpiece and the cutting edge
α_g = clearance angle as ground on the tool
ν_g = rake angle as ground on the tool
ν_n = nominal normal rake angle
θ = an intermediate angular parameter
θ_H = horizontal setting angle of type II tool
θ_V = vertical setting angle of type II tool
ξ_a = chip thickness ratio
ξ_b = chip width ratio
ξ_l = chip length ratio
ρ_c = chip flow angle
ρ_{ct} = angle between V_{ct} and the normal to the cutting edge on the rake plane
ρ_F = angle between friction force F and the normal to the cutting edge on the rake plane
τ_s, τ_r = flow stress of the work material at the shear plane and near the rake plane
ϕ_n = normal shear angle
$(\phi_l)_v$ = lateral shear angle derived from velocities
ω_n = angle between P_n and R_n

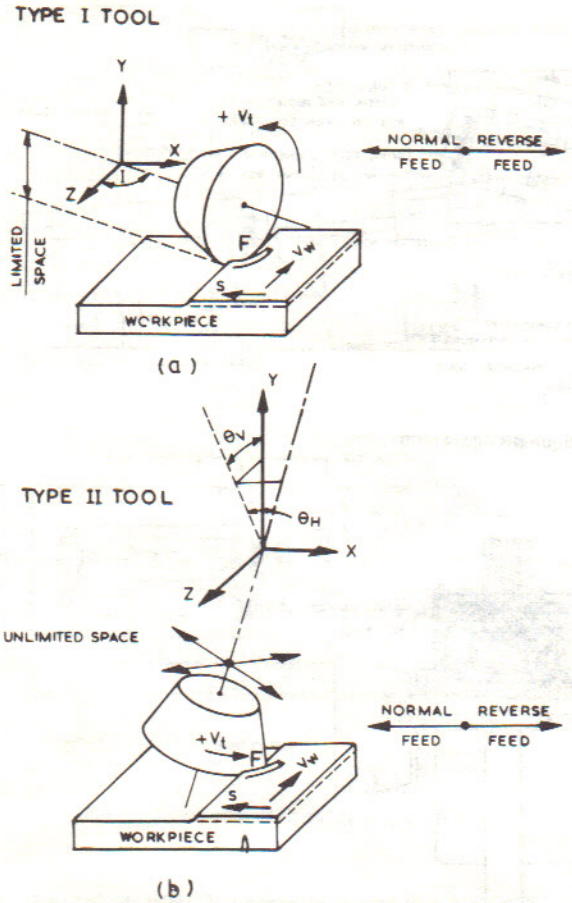

Fig. 1 Modes of cutting with rotary tools

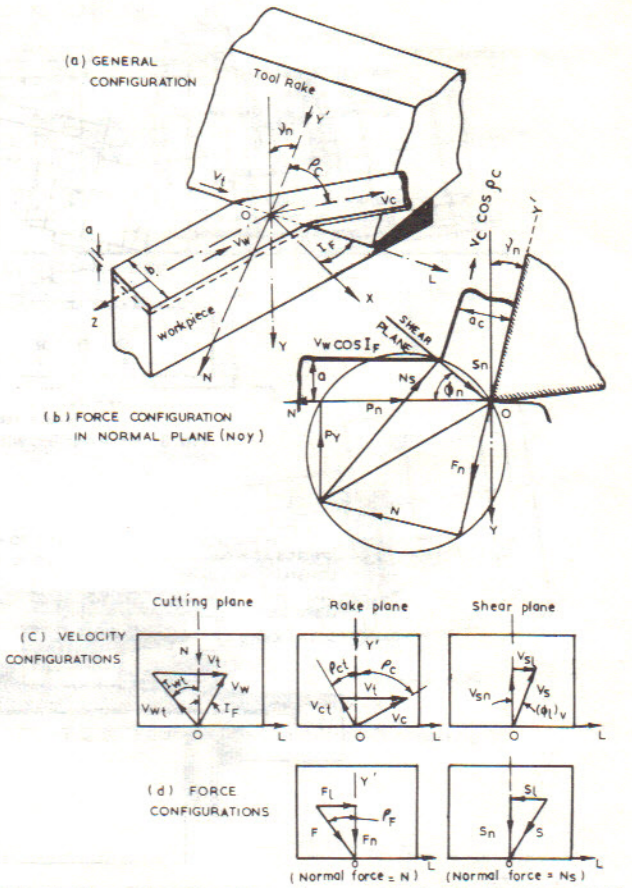

Fig. 2 General configuration of forces and velocities in oblique DRT

Test Rig II. This set up was used mainly to study chip formation at high rotary speeds. The experiments were conducted on a Kearney and Trecker Milling Machine. A HSS type II rotary tool was mounted in a special adapter fitted on the universal milling machine. The milling head permitted the necessary angle θ_H and θ_V to be set. The rest of the arrangement was similar to test rig I. This setup also included a specially constructed quick stop device illustrated in Fig. 5. The workpiece was held in a sliding block held in position by a shear pin and a clamping unit. An animal slaughtering gun was used to provide the required impact. The recoil of the gun was taken by rubber pads. The setup was initially checked by means of a displacement transducer. The chip roots were studied using photomicrography after suitably mounting, polishing and etching. Some of the chip roots were also studied for microhardness distributions using a GKN Micro Hardness Indentor.

Test Rig III. This rig was used to study the mechanics of rotary cutting in facing operations at high cutting speeds. A view of the setup is shown in Fig. 6. The experiments were performed on a 280mm swing DSG Lathe. An angular bracket was mounted in the place of tool post at the required angle. A three component dynamometer, similar to the one used in test rig I, was specially constructed. The dynamometer was so mounted on the angular bracket that its height relative to the workpiece could be adjusted with the help of a jack screw. The dynamometer and the angular bracket had cylindrical openings to accommodate the rotary spindle unit used in test rig I. A special base was clamped on to the angle bracket. The tool spindle received the drive from a 0.75 KW (1 hp) compound motor, mounted on the base, through a universal coupling and a change gear bracket. Facing experiments were conducted on mild steel workpieces of 203mm and 38mm bore held in the chuck. Thus, a wide range of cutting speeds could be covered in one stroke. All the chip dimensions, the tool and work speeds and the forces were measured.

Test Rig IV. This rig was similar to test rig II except that a HMT M-2 P milling machine was used with a strain gage type two component milling dynamometer (Lebow Model 6423-105), Philips (Model PT 1210/1211) ten channel switching and balancing unit in conjunction with a Bruel and Kjear (Model 1516) strain indicator.

Cutting was performed dry, as well as using various cutting fluids, namely, 3 percent emulsion, ILO Broach Oil, Shell Tonna Oil, Shell Tellus Oil 27, and Carbon Tetrachloride.

The experimental data were processed with the help of a computer program based on the equations given in the Appendix.

Experimental Results at Medium Rotary Speeds

Experiments were performed using test rig I on copper, aluminium (B.S. 1476 HE 9 NP) and mild steel specimens to obtain data on the effect of medium rotary speeds on the cutting process. The experiments included a wide range of inclination angles i_F cutting speeds and rotary speeds. For the sake of brevity, only some typical results are illustrated here.

Figure 7 shows the variations of ξ_a, ξ_b and ξ_l with angle i_{wt}, obtained at $i_F = 44.5$ deg during the free cutting experiments on copper. The parameters are plotted against i_{wt} (given by

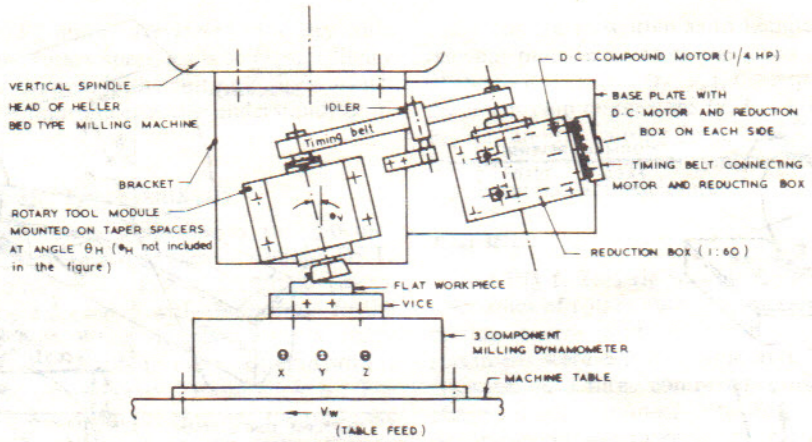

Fig. 3 Free cutting with an oblique DRT (test rig I)

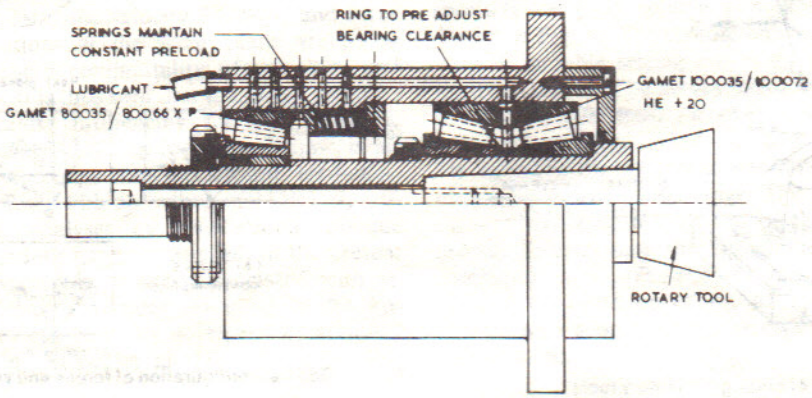

Fig. 4 Spindle unit used in test rig I

equation (A.4) in the Appendix) instead of V_t/V_w, to enable the inclusion of the entire rotary speed range of $-\infty$ to $+\infty$. The following observations may now be made.

(i) Chip length ratio ξ_l increases with an increase in rotary speed in the positive direction. At negative rotary speeds, the chip length ratio reduces. However, at very high rotary speeds, chip length ratio increases. Chip length ratios greater than unity can be obtained at high rotary speeds. $\xi_l = 2.3$ was the highest chip length ratio recorded while machining mild steel. It may be noted that such high chip length ratios have seldom been observed in conventional cutting with stationary tools.

(ii) The chip width ratio ξ_b reduces with increasing rotary speeds from negative to positive values. At high positive rotary speeds, however, there is an increasing trend of ξ_b.

(iii) The chip thickness ratio ξ_a shows a decreasing trend with increase in the rotary speed in either direction. At very high rotary speeds, there is a significant reduction in the chip thickness ratio. Values of $\xi_a < 1$ are very easily obtained in rotary machining. It may be recalled $\xi_a < 1$ is often considered to be impossible. Ultra high-speed machining [10] and machining with conventional tools oscillating in the direction of the cutting speeds [11] appear to be the only other occasions where $\xi_a < 1$ have been achieved on these work materials. Shaw, et al.'s work [7] on DRT did not report these values since the tool was orthogonal and the rotary speed ratio was limited to 2.

Figure 8 shows the variation of chip flow angle ρ_c and the normal shear angle ϕ_n. Since the tools are having an obliquity i_F, the chip flow angle when the tool was stationary ($i_{wt} = 0$) is close to angle i_F. Positive rotation of the tool carries the chip further with the tool so that the chip flow angle increases further. Usually the maximum $\rho_c = 70 - 75$ deg. Negative rotation reduces the chip flow angle. This is the reason for the observed trend of ξ_b in Fig. 7. The fall in ξ_a at high rotary speeds is due to an increase in shear angle as seen in Fig. 8. The reason for such an increase in the shear angle is explained later.

Figure 9(a) shows the variations of the measured cutting forces at $i_F = 0$ while free-cutting aluminum alloy specimens. Since $i_F = 0$, the trends in either direction of rotation of the tool are identical. It is seen that forces P_y and P_z fall enormously (up to 90 percent) at high rotary speeds. Force P_x, however, shows initially an increasing trend with rotary speed in either direction. The fall of P_z is unusual in comparison to the benefits achieved by any other technique of reducing the cutting forces. However, when the large increase in shear angle is kept in mind, this fall is understandable.

Figure 9(b), shows the variation of the cutting force components with rotary speed ratio at $i_F = 51.5$ deg. It is observed again that the forces P_y and P_z fall with an increase in rotary speed in either direction. The fall in P_z in this case is observed to be more drastic than that with $i_F = 0$ deg (Fig. 9(a)). P_z is found to become zero and even turn negative at high values of positive rotary speeds. This means that, in this condition, the tool is capable of driving the workpiece. The possibility of this was verified on test rig III by mounting the workpiece freely on centers on both sides and conducting a turning experiment at high rotary speeds. Such a situation leads to a new type of rotary tool, namely, the work propelling rotary tool (WPRT). The situation with a WPRT is exactly the reverse of that with a SPRT, where the workpiece

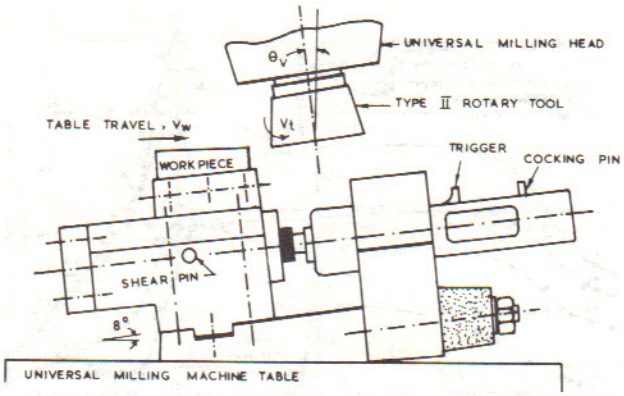

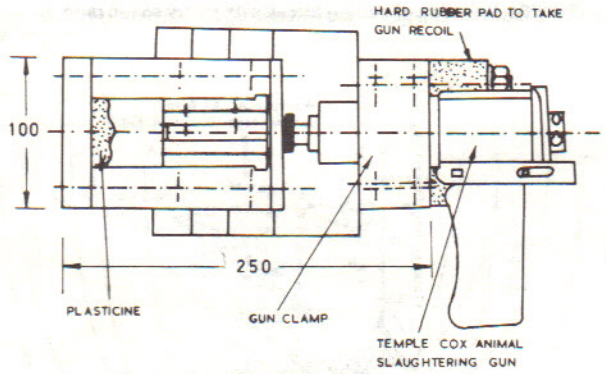

Fig. 5 Quick stop device used in test rig II

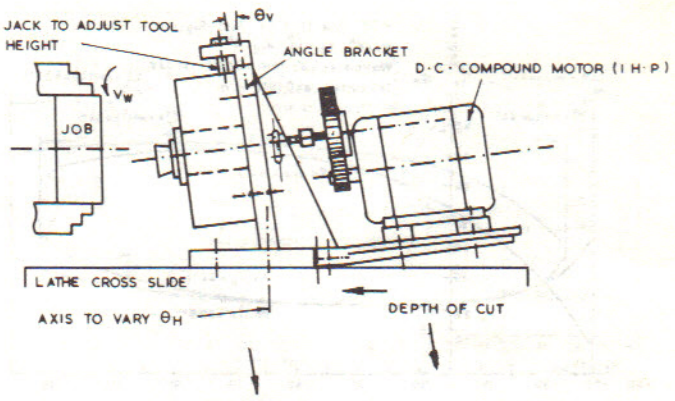

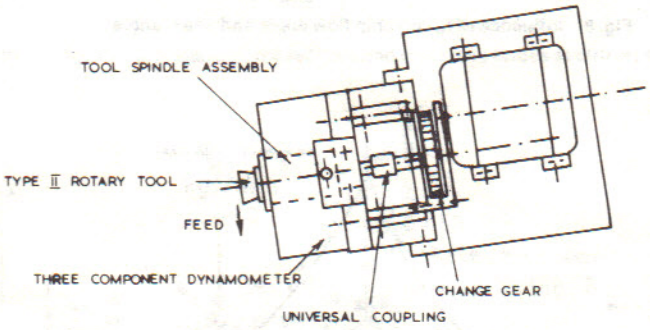

Fig. 6 Facing experiments on a lathe "test rig III"

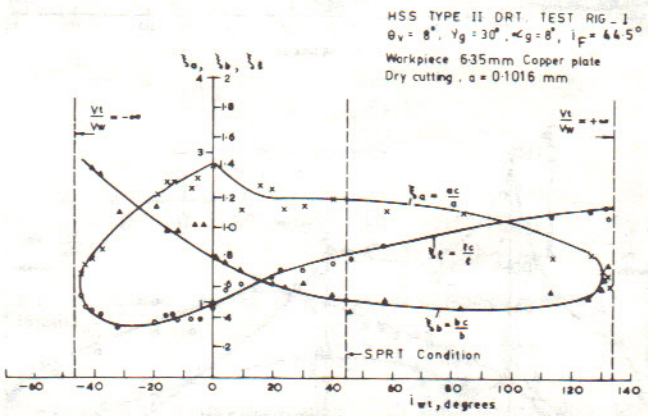

Fig. 7 Influence of i_{wt} on ξ_a, ξ_b and ξ_l

drives the tool. A WPRT inherently works at a higher V_t/V_w than that of a SPRT and results in larger shear angles and a better surface finish. The WPRT is an entirely new concept and it is too early to predict its practical potential. Comparing Figs. 9(*a*) and 9(*b*), it is noted that there is a sudden rise in forces when $i_{wt} \simeq i_F$ in Fig. 9(*b*). This is the condition of a SPRT. A close study of the nature of chips in this zone showed that the chip cross-section was triangular although the uncut section was rectangular. This indicated that a special type of chip formation is associated with SPRT which causes the observed rise in force. The triangular chips have been generally observed to be associated with low shear angles and torn machined surface. At rotary speeds away from the speed of self-propulsion, the chips obtained reverted to rectangular section.

Figure 10 shows the variation of the measured cutting forces with V_t/V_w while machining mild steel at high cutting speeds on test rig III. It is seen that the trends observed at low cutting speeds (Fig. 9(*b*)) are also observed at high cutting speeds. The sudden increase in cutting forces at the condition of SPRT is more pronounced in this case. It is also seen that the rotary speed at which P_z becomes zero is much smaller for mild steel than that for aluminium.

Figure 11 shows the variation of U/V_w (a measure of total power) with i_{wt}. It is seen that, with a proper selection of rotary speed ratio, a reduction in specific cutting energy of up to 50 percent is possible. The reduction in specific energy at medium rotary speeds is due to the influence of the rotary speed on the kinematics of chip formation and the consequent reduction in chip compression (Fig. 7). However, it is seen that the magnitude of the minimum energy is independent of i_F. Further experiments showed that the magnitude of the minimum energy decreases with increasing normal rake angle. At high rotary speeds, however, the chip is unable to follow the tool motion and starts sliding on the tool. Thus, at high rotary speeds, due to the intense sliding between the chip and the tool, the proportion of rotary energy predominates over the energy derived from the work drive and the total energy increases drastically.

Figure 12 shows the variation of the relative proportion of the energy drawn from the rotary drive to the total energy. It may be noted that the energy derived from the rotary drive is zero in two situations, viz., when $V_t/V_w = 0$ and when $V_t/V_w = (V_t/V_w)_{SPRT}$. In the former case $V_t = 0$ and in the latter case $P_l = 0$, so that $P_l V_t = 0$ in both the cases. For rotary speeds up to the speed of self propulsion, the tool acts as a brake on the work drive. Beyond the speed of self propulsion, the tool drive becomes the dominant source. The share of the rotary drive is found to increase faster with increasing values of i_F. Thus, the use of a higher value of i_F enables the beneficial effect of a DRT to be derived at lower rotary speed ratios.

Figure 13 shows the variation of the measured angular deviation ρ_F (see equation (A.17) in the Appendix) of the

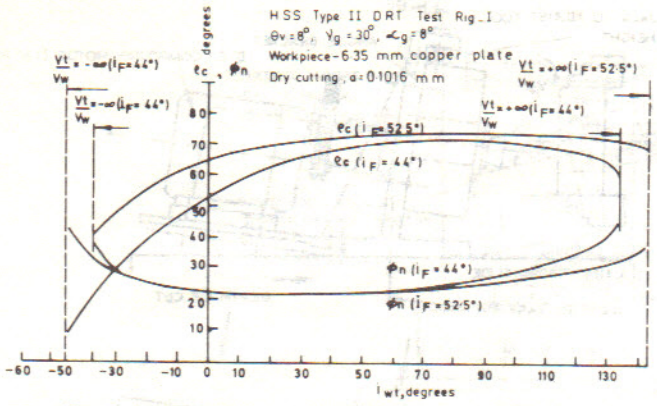

Fig. 8 Influence of i_{wt} on chip flow angle and shear angle

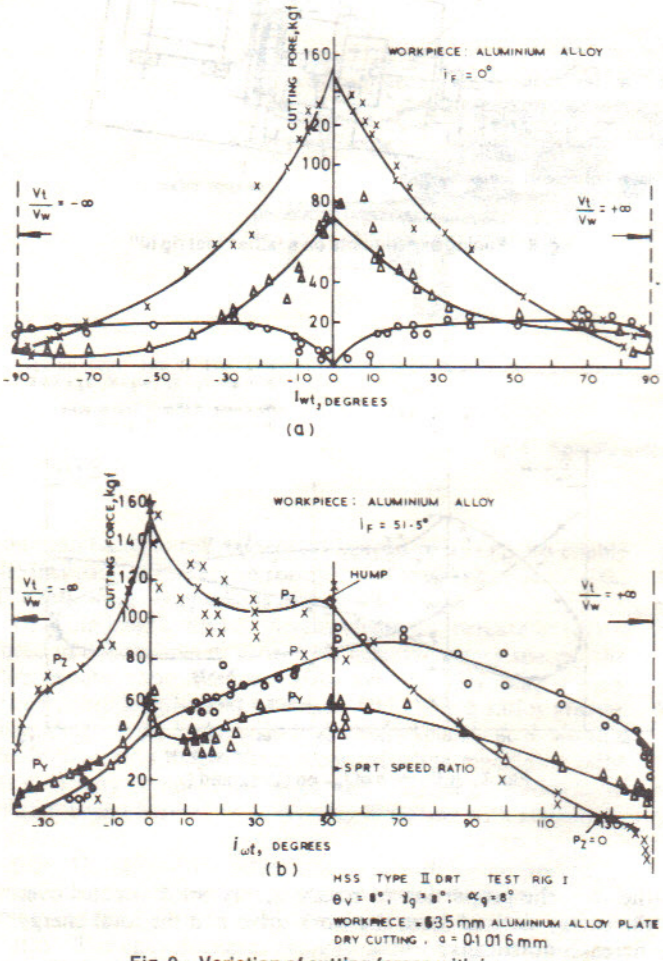

Fig. 9 Variation of cutting forces with i_{wt}

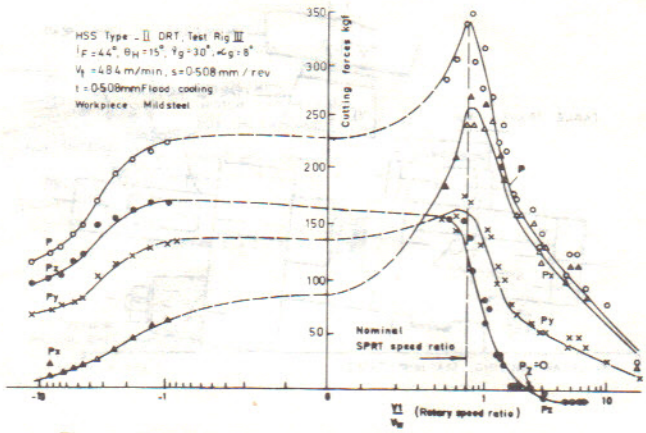

Fig. 10 Variation of cutting forces with rotary speed ratio

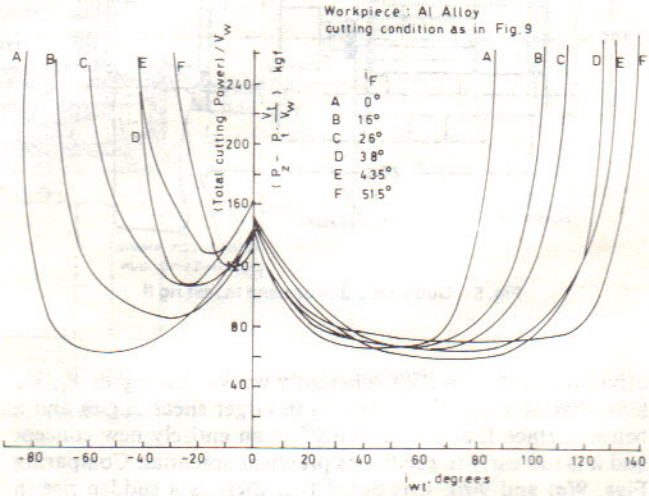

Fig. 11 Variation of total cutting power with i_{wt}

friction force F from the normal to the cutting edge on the rake surface. This angle may be interpreted as the chip flow angle estimated from the cutting forces. For the range 65 deg $> \rho_F > -40$ deg, one may write the following empirical equation:

$$\rho_F = (\rho_F)_0 - i_{wt} \tag{3}$$

where $(\rho_F)_0$ is the value of ρ_F when the tool is stationary.

In conventional oblique cutting, $i_F = \rho_F$, as per Stabler's rule [12]. Thus, an oblique DRT at moderate rotary speeds may be considered to be equivalent to a stationary oblique tool of equivalent obliquity.

$$i_{eq} = \rho_F = (\rho_F)_0 - i_{wt} \tag{4}$$

When an orthogonal DRT is used $(\rho_F)_0 = 0$ and the foregoing equation reduces to the following equation indicated by Shaw et al. [7]:

$$i_{eq} = i_{wt} = \arctan \frac{V_t}{V} \tag{15}$$

The aforesaid discussion suggests that the mechanics of cutting with a DRT at moderate rotary speeds can be analyzed by considering an equivalent oblique tool with an obliquity of i_{eq}.

Angle $(\rho_F)_0$ can be obtained by experimenting with the rotary tool held stationary so long that i_{eq} is directly determinable for any V_t/V_w through i_{wt}. In principle, it is possible to predict the cutting forces in oblique cutting once the geometry and the kinematics of chip formation are known. Such a method has been developed recently for oblique cutting using a slip line approach [13]. It is shown that

$$P_n/(\tau_s ab) = \{1 + \cos\theta\left[[(1+\cos^2\theta)/2]^{1/2} - \cos\theta + \cot\phi_n\right]\} \sec i \tag{6}$$

$$P_t/(\tau_s ab) = \sin\theta\{[(1+\cos^2\theta)/2]^{1/2} - \cos\theta + \cot\phi_n\} \sec i \tag{7}$$

where $\tan\theta = \tan i\{1 - \tan\phi_n(\sec\nu_n - \tan\nu_n)\}$ and (8)

τ_s = the flow stress on the lower boundary of the shear zone.

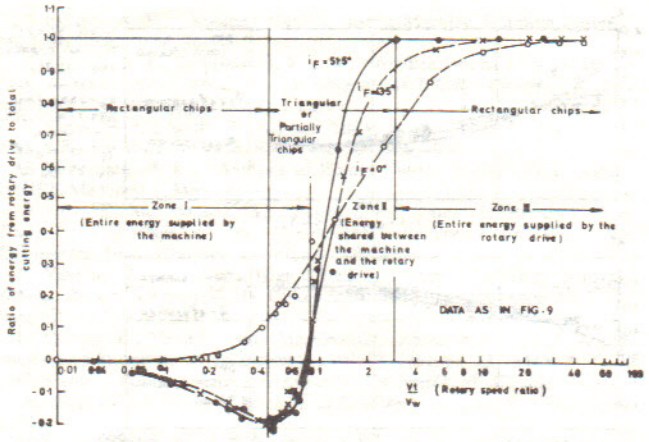

Fig. 12 Variation of energy drawn from workpiece and tool drives with V_t/V_w

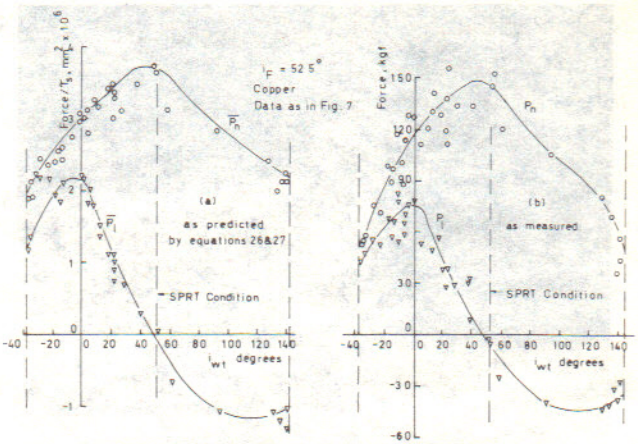

Fig. 14 Comparison of predicted and measured forces at different i_{wt}

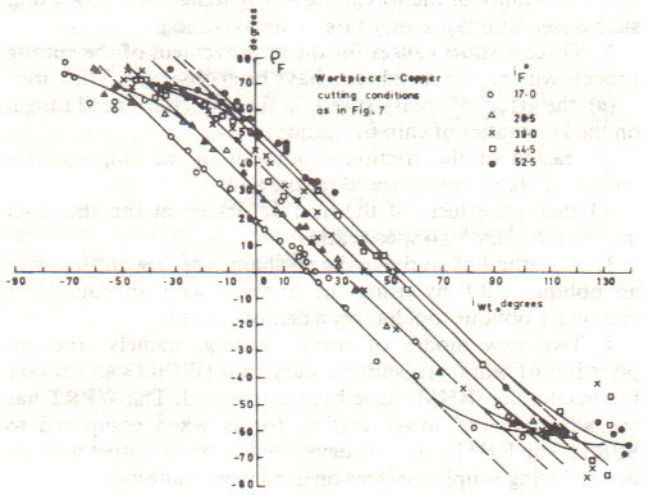

Fig. 13 Variation of chip flow angle with i_{wt}

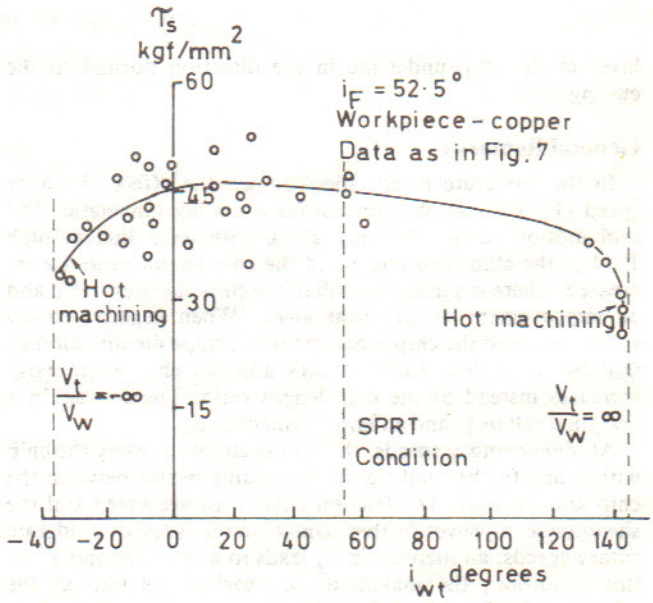

Fig. 15 Variation of shear strength of the workpiece material at different i_{wt}

For a rotary tool $i = i_{eq}$ in the foregoing equations.

Figure 14 compares the predicted variation of $P_n/\tau_s ab$ and $P_l/\tau_s ab$ with the measured trends of P_n and P_l. It is seen that the general trends have been excellently predicted by the new model of oblique cutting, in the medium rotary speed zone. The variation of flow stress τ_s on the shear plane (see equation (A.18) in the Appendix) is illustrated in Fig. 15. It is seen that in the medium rotary speed range, τ_s is fairly constant. Thus, in this range, the effect of rotary speed on the chip formation is predominantly kinematic.

Experimental Results at High Rotary Speeds

A review of Figs. 7–9, 14, and 15 shows at very high values of V_t/V_w (or i_{wt}), the natures of the variation of the different parameters are significantly different from the natures at medium rotary speeds. At high positive rotary speeds, for instance, ξ_a falls rapidly, shear angle ϕ_n increases drastically, and the cutting forces approach their minimum magnitudes. As already mentioned, at these rotary speeds, there is intense sliding between the chip and the tool and the energy derived from the rotary tool increases rapidly. The temperatures at the rake face increases enormously. Experiments on mild steel on test rigs II and IV showed that the underside of the chips could be practically made to melt. The rate of heat input compared to the flow of metal is so enormous that a large amount of heat is conducted into the shear zone so that the shear stress τ_s at the shear plane falls significantly (Fig. 15). However, the temperature at the chip tool interface is still larger than that at the shear plane so that the ratio of the flow stress τ_r at the chip tool interface to τ_s at the shear plane is reduced at high rotary speeds. Studies on microhardness distributions in the chips confirmed the foregoing. It is well known that such a situation leads to a decrease in the apparent friction angle [14] at the rake surfaces and an increase in the shear angle [15]. The rapid increase in shear angle noted in Fig. 8 at high values of $\pm i_{wt}$ is thus explained.

Figure 16 shows a photomicrograph of a chip root obtained at high rotary speeds on mild steel. The shear angle is about 53 deg and $\xi_a = 0.6$. The grain orientation in the chip is unusual. The angle between the direction of maximum elongation of grains in the chip and the shear plane is usually positive in conventional machining, whereas in Fig. 16 it is negative. The angle is positive in conventional chip formation because the process, then, is a combination of compression and shear. The negative angle in Fig. 16 suggests that the process at high V_t/V_w is a combination of tension and shear. The observation that $\xi_a < 1$ also suggests that the chip is in a state of tension. The reasons for this have recently been investigated [16]. It appears that this is caused by the squeezing out of the molten

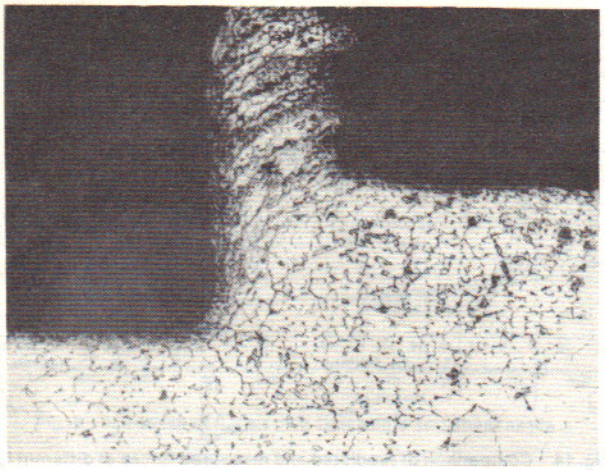

Fig. 16 Photomicrograph of a chip root obtained at high rotary speed ratio

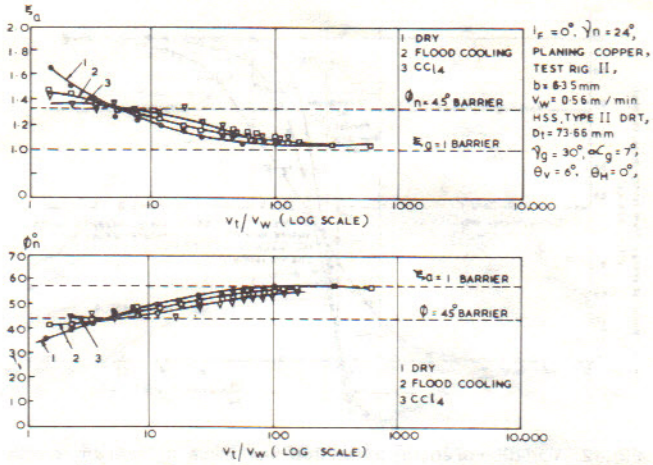

Fig. 17 Variation of ξ_a and ϕ_n with rotary speed ratio

layer at the chip underside in the direction normal to the cutting edge.

General Remarks

In the moderate rotary speed range, the effect of rotary speed (V_t/V_w) on chip formation is mainly kinematic. The tool motion carries the chip along with it so that at high V_t/V_w, the chip flow angle and the chip length ratio are increased. There is a marginal fall in the chip thickness ratio and an improvement in the shear angle. When negative rotary speeds are used the chip is carried in the opposite direction so that the chip flow angle reduces and the chip width ratio increases instead of the chip length ratio. There is again a marginal fall in ξ_c and an improvement in ϕ_n.

At higher rotary speeds, the tool is unable to carry the chip with it any further and significant sliding begins between the chip and the tool. The friction conditions are eased and the shear angle improves further. Unlike in the range of moderate rotary speeds, an increase in V_t leads to a fall in ρ_t and ξ_t. In this condition, the maximum ϕ_n reached, as well as the minimum ξ_a, have been found to be practically independent of the cutting fluid as illustrated in Fig. 17. The estimated values of ξ_t and ρ_c under the same conditions, however, exhibited significant dependence on the type of the cutting fluid. This indicates that, at high rotary speed ratios, the important effect of V_t is not kinematic, but through an easing of friction conditions at the chip tool interface.

With further increase in rotary speeds, the heat generated due to chip tool sliding predominates and a condition of hot machining sets in. The onset of hot machining condition should obviously depend on the thermal properties of the work material. Thus, on mild steel, which has a comparatively poor heat diffusivity, the temperatues could approach the melting temperature of the chip. The DRT is thus found to lead to a new type of hot machining, namely, rotary hot machining (RHM).

Conclusions

1. Experimental studies on driven rotary tools show that, with a proper selection of rotary speeds, extraordinary effects on the cutting process, namely:

(*a*) normal shear angles larger than 45 deg;

(*b*) chip length ratios as high as 2.3;

(*c*) chip thickness ratios lesser than unity;

(*d*) reduction of cutting forces down to 10 percent; and

(*e*) the cutting force component P_z becoming negative could be achieved.

The importance of the foregoing is heightened by the fact that such observations are very rare in metal cutting.

2. Three distinct causes for the improvement of the cutting process with rotary speed ratio have been observed. They are:

(*a*) the effect of rotary speed, in the moderate speed range, on the kinematics of chip formation;

(*b*) easing of the friction conditions at the chip tool interface at higher rotary speed ratios; and

(*c*) thermal effects of the heat generated at the chip tool interface at very high speed ratios.

3. A method of studying the mechanics of free cutting with an oblique DRT by using the analogy with an equivalent stationary oblique tool has been demonstrated.

4. Two new modes of rotary cutting, namely, the application of work propelling rotary tool (WPRT) and rotary hot machining (RHM) have been discovered. The WPRT has the advantage of lower cutting forces when compared to SPRT. The RHM could be developed as an effective method of producing simple surfaces on hard work materials.

5. When the present results on the DRT are combined with the earlier studies on the SPRT, it is seen that, with the proper selection of the rotary speed ratio, one can obtain any state of metal cutting at will. Thus, if reductions in temperatures and improvements in tool life are desired, the SPRT is a possible solution. If reduction in cutting forces is desired, the DRT may be used. Extremely hard work materials may be machined by taking advantage of RHM.

It is hoped that the conclusions of the present work would stimulate new applications of the rotary principle in metal cutting.

Acknowledgments

The authors thank the late Prof. F. Koenigsberger and Dr. G. Barrow for the help rendered during the investigations. The authors also thank Regional Engineering College, Warangal, and College of Engineering, Osmania University, Hyderabad, India, for their assistance.

References

1 Venuvinod, P. K., "An Investigation to Explain and Evaluate the Performance of a Rotary Tool," M. Tech. dissertation, I.I.T., Bombay, 1965.

2 Venuvinod, P. K., Somasundaram, S., and Ramaswamy Iyer, N., "Rotary Tools," Machine Building Industry, India, Mar. 1966.

3 Zemlyanskii, V. A., "Wear of Circular Self Rotating Tools Expressed as a Function of the Path of Travel of Cutting Edge on the Workpiece," *Samoletostoroenie i Tekhnika Vozdushnoga Flota*, Kharkov, Part 3, 1965, pp. 86-91.

4 Granin, Yu. F., "Wear and Life of Circular Self Rotating Tools," *Samoletostroenie i Tekhnika Vozdushnoga Flota*, Kharkov, Part 2, 1965, pp. 106-111.

5 Eskelin, A. F., "Rotating Carbide Inserts Machine Titanium Faster," Machinery, Dec. 1966, 96–98.
6 Thomas, R. L., and Lawson, R. L. J., "Applications of Rotary Turning Tools," *Proceedings of 16th International M.T.D.R. Conference*, Birmingham, Sept. 1976, pp. 125–131.
7 Shaw, M. C., Smith, P. A., and Cook, N. H., "The Rotary Cutting Tool," TRANS. ASME, Vol. 74, Aug. 1952, pp. 1065–1976.
8 Venuvinod, P. K., "Analysis of Rotary Cutting Tools," Ph.D. thesis, UMIST, Manchester, May 1971.
9 Kasei, K., and Masuda, M., "Research on Turning with Rotary Cutting Tools," *Proceedings of the International Conference on Production Engineering*, New Delhi, Vol. I, 1977, pp. 214–223.
10 Vaughn, R. L., "Ultra High Speed Machining (Feasibility Study)," A.M.C. Report, TR 66-7-635(1), United States Air Force, Patterson Air Force Base, Ohio, 1959.
11 Hitomi, K., "Fundamental Machinability Research in Japan," ASME JOURNAL OF ENGINEERING FOR INDUSTRY, Vol. 83, 1961, pp. 531–544.
12 Stabler, G. V., "The Fundamental Geometry of Cutting Tools," *Proceedings of Institution of Mechanical Engineers*, London, Vol. 165, 1951, p. 14.
13 Venuvinod, P. K., Lau W. S., and Barrow, G., "A New Model of Oblique Cutting," Paper No. 77-WA&Prod-6, presented at the Winter Annual Session of ASME, Atlanta, USA, Nov. 1977, and published in TRANS. ASME, Vol. 100, No. 2, 1978.
14 Loladze, T. N., "Problems of Determining Stress at Cutting Edge of a Tool," *Proceedings of Theoretical and Applied Mechanics Congress*, Bombay, 1961.
15 Oxley, P. L. B., and Hatton, A. P., "Shear Angle Solution Based on Experimental Shear Zone and Tool-Chip Interface Stress Distributions," *International Journal of Mech. Science*, Vol. 5, 1963, p. 41.
16 Venuvinod, P. K., and Reddy, P. N., "Investigations into Rotary Hot Machining," Unpublished Report, Regional Engineering College, Warangal, India/Hong Kong Polytechnic, Hong Kong, 1979.

APPENDIX

Equations Relating the Various Parameters Involved in Free Cutting With an Oblique DRT

$$\xi_a = \frac{a_c}{a}, \xi_b = \frac{b_c}{b}, \xi_l = \frac{l_c}{l} \qquad \text{(A.1 } a,b,c\text{)}$$

$$\cos \rho_c = \xi_b \cos i_F \qquad \text{(A.2)}$$

$$\tan \phi_n = \frac{\cos \nu_n}{\xi_a - \sin \nu_n} \qquad \text{(A.3)}$$

$$\tan i_{wt} = \frac{\frac{V_t}{V_w} \cos i_F}{1 - \frac{V_t}{V_w} \sin i_F} \qquad \text{(A.4)}$$

$$V_c = \xi_l V_w \qquad \text{(A.5)}$$

$$V_{ct} = \frac{V_c \cos \rho_c}{\cos \rho_{ct}} \qquad \text{(A.6)}$$

$$\tan \rho_{ct} = \frac{V_t - V_c \sin \rho_c}{V_c \cos \rho_c} \qquad \text{(A.7)}$$

$$\tan (\phi_l)_v = (\tan i_F - \xi_l \sin \rho_c) \frac{\cos (\phi_n - \nu_n)}{\cos \nu_n} \qquad \text{(A.8)}$$

$$V_s = \frac{V_w \cos i_F \cos \nu_n}{\cos (\phi_n - \nu_n) \cos (\phi_l)_v} \qquad \text{(A.9)}$$

$$P_n = P_z \cos i_F + P_x \sin i_F \qquad \text{(A.10)}$$

$$P_l = P_z \sin i_F - P_x \cos i_F \qquad \text{(A.11)}$$

$$S_l = F_l = P_l \qquad \text{(A.12)}$$

$$S_n = P_n \cos \phi_n - P_y \sin \phi_n \qquad \text{(A.13)}$$

$$N_s = P_n \sin \phi_n + P_y \cos \phi_n \qquad \text{(A.14)}$$

$$F_n = P_n \sin \nu_n + P_y \cos \nu_n \qquad \text{(A.15)}$$

$$N = P_n \cos \nu_n - P_y \sin \nu_n \qquad \text{(A.16)}$$

$$\tan \rho_F = F_l / F_n \qquad \text{(A.17)}$$

$$\tau_s = \frac{S \sin \phi_n \cos i_F}{ab} \qquad \text{(A.18)}$$

$$U = U_w + U_t = P_z V_w + P_l V_1 \qquad \text{(A.19)}$$